HHS Public Access

Author manuscript

J Biomech. Author manuscript; available in PMC 2019 March 01.

Published in final edited form as:

J Biomech. 2018 March 01; 69: 10–18. doi:10.1016/j.jbiomech.2018.01.016.

Mechanical Properties of Porcine Brain Tissue *In Vivo* and *Ex Vivo* Estimated by MR Elastography

Charlotte A. Guertler[1], **Ruth J. Okamoto**[1], **John L. Schmidt**[1], **Andrew A. Badachhape**[2], **Curtis L. Johnson**[3], and **Philip V. Bayly**[1,2]

[1]Washington University in St. Louis, Mechanical Engineering and Materials Science

[2]Washington University in St. Louis, Biomedical Engineering

[3]University of Delaware, Biomedical Engineering

Abstract

The mechanical properties of brain tissue *in vivo* determine the response of the brain to rapid skull acceleration. These properties are thus of great interest to the developers of mathematical models of traumatic brain injury (TBI) or neurosurgical simulations. Animal models provide valuable insight that can improve TBI modeling. In this study we compare estimates of mechanical properties of the Yucatan mini-pig brain *in vivo* and *ex vivo* using magnetic resonance elastography (MRE) at multiple frequencies. MRE allows estimations of properties in soft tissue, either *in vivo* or *ex vivo*, by imaging harmonic shear wave propagation. Most direct measurements of brain mechanical properties have been performed using samples of brain tissue *ex vivo*. It has been observed that direct estimates of brain mechanical properties depend on the frequency and amplitude of loading, as well as the time post-mortem and condition of the sample. Using MRE in the same animals at overlapping frequencies, we observe that porcine brain tissue *in vivo* appears stiffer than brain tissue samples *ex vivo* at frequencies of 100 Hz and 125 Hz, but measurements show closer agreement at lower frequencies.

Keywords

Magnetic resonance elastography; Brain tissue stiffness; Shear modulus; Post-mortem tissue changes; Porcine brain

1. Introduction

Traumatic brain injury (TBI) occurs when sudden head acceleration leads to shearing and stretching of brain tissue (Holbourn, 1943; Sierra et al., 2015). It is the leading cause of

Corresponding Author: Charlotte Guertler, Washington University in St. Louis, Mechanical Engineering and Materials Science, Urbauer 319, Campus Box 1185, 1 Brookings Drive, St. Louis, Missouri 63130, TEL: 508-259-4535, charlotte.guertler@wustl.edu.

7. Conflict of Interest Statement

None of the authors have a conflict of interest that could influence the work described in this manuscript.

death in children and young adults (Langlois et al., 2006) and is common among soldiers exposed to explosive blast in combat (Hoge et al., 2008). Computer models can be used to simulate TBI, particularly the mechanics of fast brain deformation. Simulations can be used to improve methods for injury prevention, diagnosis, and treatment. However, computer models of TBI require accurate material properties for brain tissue (Sierra et al., 2015).

The mechanical behavior of the brain remains incompletely characterized (Chatelin et al., 2010). Most mechanical testing of brain tissue is performed using animal tissue *ex vivo* (Arbogast and Margulies, 1998; Bilston et al., 1997; Brands et al., 2000; Hrapko et al., 2006; Nicolle et al., 2004; Ommaya, 1968; Shen et al., 2006; Thibault and Margulies, 1998; Vappou et al., 2007). However, *ex vivo* measurements may not necessarily reflect *in vivo* behavior (Miller et al., 2000; Rashid et al., 2012). *In situ* and *in vivo* tests have also been performed using indentation on animals (Gefen and Margulies, 2004; Miller et al., 2000) and magnetic resonance elastography (MRE) on both animals and humans (Clayton et al., 2011; Feng et al., 2013a; Johnson et al., 2016; Papazoglou et al., 2008; Schregel et al., 2012). Substantial differences have been found between estimates of material parameters, likely due to differences in methodology, frequency range, or time scale.

The relationship between *in vivo* and *ex vivo* properties of brain tissue remains a topic of active research (Gefen and Margulies, 2004). Bilston et al. (2001) hypothesized that brain tissue properties *in vivo* would be stiffer than properties *ex vivo*. Miller et al. (2000) performed one *in vivo* indentation test on exposed porcine brain and found stiffness measurements on the same order of magnitude as *in vitro* data. Gefen and Margulies (2004) compared mechanical properties in the porcine brain *in vivo* to corresponding properties post-mortem, *in situ* (i.e., after death, but in the intact head), and *ex vivo* (in the extracted brain), also using indentation. These studies found *in vivo* shear moduli stiffer than moduli measured post-mortem on preconditioned tissue (either *in situ* or *ex vivo*). Although these results offer insight into the relationship between *in vivo* and *ex vivo* tissue mechanical properties, the methods have important limitations. Indentation of the intact brain only measures properties near the surface. Also, indentation is sensitive to the detection of contact, and, unless performed at multiple speeds, provides limited information on frequency/strain-rate dependence. Dynamic shear testing of thin tissue samples (Arbogast and Margulies, 1998; Feng et al., 2013b; Hrapko et al., 2006) has been widely used for material characterization. Shear testing assumes flat samples, constant normal force, no slip, and affine deformations; conditions which are rarely satisfied. Furthermore, dynamic shear testing is impractical for *in vivo* tissue.

MRE is an imaging technique for non-invasively measuring the mechanical properties of soft tissue (Muthupillai et al., 1995). In MRE, shear waves are induced in tissue by harmonic mechanical actuation, and imaged with a modified MR imaging sequence that includes harmonic, motion-sensitizing gradients. The material properties of tissue can be calculated using local wavelength estimation, direct inversion of the viscoelastic shear wave equation, or finite element methods (Manduca et al., 2001). While deformations are typically small (<0.1% strain) the linear, viscoelastic properties that govern behavior in this regime are important and complement parameters that describe large-amplitude, quasi-static response. MRE has been used to characterize tissues like brain, liver, and muscle *in vivo* and to study

changes in stiffness due to aging, disease, or injury (Klatt et al., 2007; Riek et al., 2011; Sack et al., 2011, 2009b; Sinkus et al., 2005). However, estimates of brain properties obtained by MRE (Atay et al., 2008; Johnson et al., 2013; Sack et al., 2009a; Vappou et al., 2008, 2007) tend to differ from estimates of properties measured *ex vivo* by direct mechanical tests (Feng et al., 2013b; Hrapko et al., 2006; van Dommelen et al., 2010; Vappou et al., 2007). It is not clear whether conflicting estimates arise from differences in methodology or actual properties.

Still lacking are direct comparisons between dynamic mechanical properties estimated throughout the brain by the same method at similar frequencies and amplitudes, both *in vivo* and *ex vivo*. In this study, we address this need by performing MRE on porcine brain tissue over a range of frequencies, obtaining stiffness estimates both *in vivo* and *ex vivo* within the same tissue volume.

2. Methods

In vivo and *ex vivo* anatomical MRI and MRE scans were performed on six Yucatan mini-pigs (age range: 4 to 8 months; weight range: 23 to 50 kg). The experimental protocol was approved by the Washington University in St. Louis Animal Studies Committee, and all studies were supervised by veterinary staff.

2.1 *In vivo* Scanning

All scans were performed on a Siemens Prisma® 3T MRI scanner at Washington University in St. Louis. The mini-pigs were anesthetized with Telazol Ketamine Xylazine (TKX). An IV catheter and endotracheal tube were placed prior to scanning. Anesthesia was maintained with isoflurane via endotracheal tube. Temperature, pulse, respiration, and SPO_2 were monitored. Mini-pigs were scanned in either ventral or dorsal recumbency. For dorsal recumbency (4 animals), the animal was positioned with its back on the scanner table (Figure 1A), and its head was placed in the base of the Siemens Head/Neck 20 coil. A combination of padding and Velcro™ straps was used to secure the head. For ventral recumbency (2 animals), the animal was positioned with its stomach on the scanner table. Its head was placed under a custom half-dome Plexiglas frame (Figure 1C); a combination of padding and Velcro™ straps was used to secure the head. The Siemens 18-channel Body Matrix Coil was fastened on the Plexiglas frame and MR table using Velcro™ straps.

A custom multi-directional jaw actuator was designed to transmit harmonic motion from a pneumatic driver into the porcine brain while minimizing dissipation from muscle and fat. The actuator was fabricated from two small, empty plastic bottles (Figure 1A.1). A custom Delrin (Acetal) holder fit around the tube/bottle neck connections of each bottle. Two holes on each side of the Delrin holder secured an elastic Velcro™ nose strap. Two rubber timing belts encircling each bottle provided traction between the bottles and mini-pig molars (Figure 1A and 1C). After positioning the mini-pig head in the coil, the custom actuator was placed inside the jaw, with the bottles between the rear molars. The nose strap was tightened around the upper and lower jaws to minimize slippage between the teeth and actuator.

T1-weighted ("MP-RAGE") and T2-weighted MR images were taken at the beginning of every *in vivo* MR scanning session (Figures 1B, 1D; Figure 2A). Image volumes were acquired at 0.8 mm^3 or 0.9 mm^3 isotropic resolution for an in-plane field of view of 205 mm x 205 mm (0.8 mm^3 res) or 230 mm x 230 mm (0.9 mm^3 res). A total of 192 (0.8 mm^3 res) or 96 (0.9 mm^3 res) slices were taken for each scan. Two averages were done for each image set. The anterior-posterior direction of the image volumes was aligned with the genu-splenium axis of the corpus callosum. The total scan time for the two anatomical acquisitions was 21 minutes.

For MRE, the skull was vibrated at frequencies of 50 Hz, 80 Hz, 100 Hz, or 125 Hz using a commercially available pneumatic driver (Resoundant™ Rochester, MN) connected to the custom jaw actuator (Table 1). MRE data with 3D displacement components, each encoded by image phase, were acquired with a 2D multi-shot spiral sequence (Johnson et al., 2013) with 1.5 mm isotropic voxels covering a volume of 180 x 180 x 60 mm^3. One vibration frequency was used per acquisition. Multiple sinusoidal motion-encoding cycles of gradient strength 30 mT/m were synchronized with motion to induce phase contrast proportional to displacement (2.45 microns/rad at 50 Hz and 100 Hz, 3.91 microns/rad at 80 Hz, and 3.06 microns/rad at 125 Hz) (Atay et al., 2008). Data for each mini-pig were collected over 2–3 scanning sessions using 1–3 actuation frequencies per session.

MRE data were phase-unwrapped using open-source software FSL Prelude (Smith et al., 2004). Voxels in the MRE volume were fitted to a model of rigid-body displacement and these rigid-body effects were removed to isolate displacements due to wave motion (Badachhape et al., 2017).

2.2 *Ex vivo* Scanning

Ex vivo scanning of tissue from the same six Yucatan mini-pig brains was performed on an Agilent/Varian DirectDrive 4.7T small-bore animal MRI scanner at room temperature (~21°C). Once all *in vivo* scanning was complete, the mini-pigs (aged 6–9 months) were euthanized by barbiturate overdose. (Note: ages differ from *in vivo* scans because multiple *in vivo* scans were performed on each mini-pig over 2–4 months; 0–2 weeks elapsed between the last *in vivo* scan and the *ex vivo* scan). The brain was immediately extracted following euthanasia and dissected to expose the inferior section of the corpus callosum. A cylindrical sample containing the corpus callosum and superior gray matter, 42 mm in diameter, was extracted from the brain using a cylindrical punch. The sample was embedded in gelatin made with 2:1:1 glycerol, water, and pre-buffered saline (PBS) in a 45 mm cylindrical container (Schmidt et al., 2016) (Figure 1E). Ex vivo scans began within 2 hours post-mortem.

Ex vivo samples were vibrated at frequencies of 80 Hz, 100 Hz, 125 Hz, 200 Hz, and 300 Hz (Table 1). Shear waves were excited by a central actuation rod of 3 mm diameter that punctured the center of the sample (Figure 1E). This rod was driven harmonically by an MR-compatible piezoelectric actuator (APA150M, Cedrat Technologies, Meylan, France). Anatomical images were taken at 1 mm isotropic resolution with a field of view of 48 x 48 x 25 mm^3 (Figure 1F, Figure 2B). Images were obtained at TE of 60 ms. MRE data were acquired with a modified 2D multi-slice spin-echo sequence with 1 mm isotropic voxels, TR

= 1000–1200 ms, and TE = 28–40 ms covering a volume of 48 x 48 x 25 mm^3 (Figure 1F). Sinusoidal motion-encoding gradients (1–3 cycles) of amplitude 100–120 mT/m were synchronized with motion to induce phase contrast proportional to displacement (7.48 microns/rad at 80 Hz (n=1), 100 Hz (n=2), 200 Hz (n=5), and 300 Hz (n=5) and 9.35 microns/rad at 100 Hz (n=3), 125 Hz (n=2), 200 Hz (n=1), and 300 Hz (n=1)). MRE data were phase-unwrapped and rigid-body motion effects were removed using the methods detailed in section 2.1.

2.3 Local Direct Inversion

Local direct inversion (LDI) was performed on both the *in vivo* and *ex vivo* MRE displacement fields to estimate the mean complex shear modulus of the mini-pig brain sample at each of the measured frequencies using the viscoelastic analog to the Navier equation (Okamoto et al., 2011):

$$(G^{'}+iG^{''})\nabla^2\boldsymbol{U}(x,y,z)=-\rho\omega^2\boldsymbol{U}(x,y,z), \quad (1)$$

where the complex vector $\boldsymbol{U}(x, y, z)$ contains the Fourier coefficients of the fundamental harmonic of the 3D displacement field, $G^{'}$ is the storage modulus, and $G^{''}$ is the loss modulus. This equation assumes that the material is linear, isotropic, and locally homogeneous.

Estimates of storage and loss moduli were obtained for the entire brain *in vivo* and the entire sample of *ex vivo* brain and gelatin. Voxel-wise estimates were averaged over a region of interest (ROI) corresponding to the location and dimensions of the *ex vivo* brain samples. Storage modulus maps were further eroded using a 7x7x7 kernel to remove the possible effects of neighboring gelatin on the averaged storage modulus estimates in the *ex vivo* tissue.

3. Results

Figure 3 shows examples of wave displacement, shear strain, and curl for one axial slice of the porcine brain *in vivo*. Although displacement components exist in all three directions, the out-of-plane, anterior-posterior (AP, z) component of motion (u_z) is the dominant component excited by the custom actuator. The displacement amplitude is ~1.5 μm. The curl of the wave field, which isolates the contribution of shear waves, is dominated by the component along the right-left (RL, x) axis, $\Gamma_x=\frac{\partial u_y}{\partial z}-\frac{\partial u_z}{\partial y}$. Shear strain and curl have similar magnitude (~2×10^{-4}); the most prominent component of the strain tensor is $\varepsilon_{zy}=\frac{\partial u_y}{\partial z}+\frac{\partial u_z}{\partial y}$.

Figure 4 shows examples of displacement, shear strain, and curl maps for one coronal slice of porcine brain tissue *ex vivo*. The dominant displacement component (~15 μm amplitude) during shear wave propagation is in the out-of-plane (u_z) direction, which is the superior-inferior (SI) direction with respect to the brain. The curl of the wave field shows that the propagation of the waves occurs radially outward in the xy-plane. The largest components of curl and strain are ~2×10^{-3} mm/mm, which are well within the small-deformation regime.

Figure 5 displays storage modulus estimates for four representative *in vivo* axial slices spaced 7.5 mm apart and one representative *ex vivo* coronal slice estimated using LDI for the data taken at 100 Hz. The *ex vivo* sample is surrounded by the gelatin, which is represented by the less stiff (~1 kPa) estimates in the image.

To compare property estimates *in vivo* and *ex vivo*, an ROI was defined in the *in vivo* image volume to match the dissected sample used in *ex vivo* scanning. The ROI (Figure 6) is a 42 mm cylinder that includes the corpus callosum and superior regions. To remove the effects of the gelatin surrounding the *ex vivo* sample and the estimates near the actuator rod, the ROI for the *ex vivo* stiffness data was eroded using the MATLAB *imerode* command (2014a, MathWorks, Natick, MA) with a 7x7x7 kernel.

Figure 7 displays histograms of LDI estimates of storage modulus (G') values for all voxels from the ROI of the *in vivo* image volume and from the eroded ROI of the *ex vivo* sample from all scans performed at 100 Hz and 125 Hz. The mean for each data set is depicted by the dashed line. These histograms show (i) higher stiffness at the higher frequency, and (ii) *in vivo* tissue is stiffer than *ex vivo* tissue. The effect of orientation (dorsal or ventral) *in vivo* on brain stiffness was checked, and found to be small (voxelwise mean ± std.: 0.779 ± 0.347 kPa dorsal vs. 0.777 ± 0.468 kPa ventral for 50 Hz; 2.264 ± 0.649 kPa vs. 2.381 ± 0.820 kPa for 100 Hz).

At each frequency, the mean storage and loss moduli from the ROI of the *in vivo* image volume were estimated, along with the corresponding mean storage and loss moduli in the eroded ROI of the *ex vivo* image volume. The means and standard deviations of these parameters are plotted versus frequency in Figure 8. Both *in vivo* and *ex vivo* estimates of storage modulus increase with frequency. Notably, estimates of storage modulus are higher for the *in vivo* data than for the *ex vivo* data at all common frequencies. Multivariate regressions of storage and loss moduli were performed using a linear mixed-effects model with random subject effects. Group (*in vivo* vs. *ex vivo*), frequency, and their interaction were the independent predictors (Appendix B). For storage modulus, the slopes between *in vivo* and *ex vivo* were significantly different ($p < 0.0001$) and frequency was a good predictor of the data ($p < 0.0001$). No significant differences were observed between loss moduli *in vivo* and *ex vivo* over this frequency range ($p = 0.285$). The linear mixed-effects model is included with mean storage and loss modulus estimates, in Figure 8. Storage and loss modulus estimate were also fitted to several candidate rheological models (Appendix C).

4. Discussion

This study provides the first comparison of *in vivo* and *ex vivo* material properties throughout a volume of brain tissue in the same large animal using MRE. MRE was performed on brain tissue both *in vivo* and *ex vivo* at multiple frequencies, illuminating the viscoelastic behavior of brain tissue under both conditions. MRE estimates of storage modulus suggest that tissue in the intact, living brain is stiffer than in *ex vivo* samples. Direct comparison was possible at overlapping frequencies of 80 Hz, 100 Hz, and 125 Hz.

Estimates in *ex vivo* tissue at other frequencies (200 Hz, and 300 Hz) support this general observation.

MRE in pigs is quantitatively similar to MRE in humans. In Figure 3 the magnitude of wave displacement *in vivo* is on the order of 1–2 microns, similar to magnitudes observed in human studies *in vivo* using a “pillow” actuator (Badachhape et al., 2017) or “paddle” actuator (Clayton et al., 2012). The largest component of wave motion in the current *in vivo* studies is in the AP direction. Larger amplitudes are achieved in the *ex vivo* sample since waves are excited by direct vibration of the tissue; the largest component of wave motion is in the SI direction.

Our estimates of storage modulus *ex vivo* at 80 Hz are within 15% of several estimates from the literature on the porcine brain taken using MRE (Vappou et al., 2007) or oscillatory shear strain at 2.5% (Arbogast and Margulies, 1997; Thibault and Margulies, 1998). At higher frequencies, the current *ex vivo* estimates of storage modulus are greater than prior estimates in porcine brain and exhibit a steeper dependence on frequency (Arbogast and Margulies, 1997; Thibault and Margulies, 1998; Vappou et al., 2007). Current estimates of loss modulus for *ex vivo* are lower than prior estimates (Arbogast and Margulies, 1997; Thibault and Margulies, 1998; Vappou et al., 2007).

What might explain the observed mechanical differences between *in vivo* and *ex vivo* brain tissue? *Ex vivo* tissue experiences neither perfusion nor metabolic activity, and any residual stress in *ex vivo* tissue is relieved by dissection. More comprehensive studies are needed to determine which factors might explain observed stiffness differences.

It is possible that anisotropy of white matter might have contributed to differences between *in vivo* and *ex vivo* parameter estimates (Anderson et al., 2016; Schmidt et al., 2016; Tweten et al., 2015). Anderson et al. (2016) found ~20% differences in estimated storage modulus of white matter between areas where displacements were primarily parallel vs. perpendicular to the dominant fiber direction. In the current study, although the dominant tissue motions were in different anatomical directions *in vivo* and *ex vivo*, in both cases tissue displacements were perpendicular to the dominant (right-left) fiber direction. Tissue motion *in vivo* was primarily anterior-posterior (Figure 3) and tissue motion *ex vivo* was primarily superior-inferior (Figure 4); both are perpendicular to the fiber axis. Also, differences between *in vivo* and *ex vivo* estimates diminish at low frequencies. Thus, anisotropy is unlikely to explain the observed differences.

Temperature affects tissue properties. We did not monitor the sample temperature in the current *ex vivo* studies, but in prior studies with gelatin samples (Okamoto et al., 2011) sample temperature during MRE was ~21°C, which is substantially lower than *in vivo* (~37°C). However, in viscoelastic tissue lower temperatures are typically associated with higher storage modulus (Hrapko et al., 2008), which would tend to mask observed differences.

The pig brain *in vivo* is surrounded by CSF and skull; *ex vivo* tissue was encased in gelatin in a plastic container. Boundaries should have minimal effects in both cases because we analyzed only interior ROIs removed from the boundaries. Also, differences in estimated

properties are greater at higher frequencies, at which the effects of boundaries are likely less important, due to shorter wavelengths.

Future studies could investigate *ex vivo* brain tissue *in situ* (i.e., in the intact head post mortem) to account for factors related to tissue extraction. However, the logistical challenges of doing *in vivo*, *in situ*, and *in vitro* MRE in the same animal are substantial.

Other limitations exist for both *in vivo* and *ex vivo* experiments. Since the porcine brain is small (~100 g), images are at a lower resolution, relative to brain anatomical structures, than typical human scans. Due to differences in actuation and sample geometry, the frequency ranges for *in vivo* and *ex vivo* studies did not overlap completely. The mini-pig head *in vivo* has thick layers of bone, fat and muscle, so that frequencies above 125 Hz dissipated before reaching the brain. In the *ex vivo* sample, below 80 Hz, insufficient wavelengths were obtained for accurate parameter estimation. Strain amplitudes were higher in *ex vivo* experiments, though in both *in vivo* and *ex vivo* samples strains were < 0.2%, well within the small-strain (linear) regime. Differences between *in vivo* and *ex vivo* studies and data characteristics are summarized in Appendix A.

5. Conclusion

This study shows notable differences between material properties estimated by MRE *in vivo* and *ex vivo* in similar volumes of brain tissue from the same animal, over multiple frequencies. Although many *ex vivo* measurements of brain tissue mechanical properties are available, only limited data have been obtained *in vivo*. Thus, most TBI simulations incorporate material parameters measured *ex vivo*. The current results thus represent progress toward accurate simulation of TBI in the intact, living brain.

Supplementary Material

Refer to Web version on PubMed Central for supplementary material.

Acknowledgments

This study was performed with funding from NIH Grant R01 NS055951, NSF Grant CMMI-1332433, ONR Grant N00014-15-C-5160, and Imaging Sciences Pathway Fellowship NIH 5T32EB01485505. Technical assistance from Linda Hood in MR image acquisition is gratefully acknowledged.

References

Anderson AT, Van Houten EEW, McGarry MDJ, Paulsen KD, Holtrop JL, Sutton BP, Georgiadis JG, Johnson CL. Observation of direction-dependent mechanical properties in the human brain with multi-excitation MR elastography. J Mech Behav Biomed Mater. 2016; 59:538–546. DOI: 10.1016/j.jmbbm.2016.03.005 [PubMed: 27032311]

Arbogast KB, Margulies SS. Material characterization of the brainstem from oscillatory shear tests. J Biomech. 1998; 31:801–807. DOI: 10.1016/S0021-9290(98)00068-2 [PubMed: 9802780]

Arbogast, KB., Margulies, SS. Regional Differences in Mechanical Properties of the Porcine Central Nervous System. Proceedings of the 41st Stapp Car Crash Conference; 1997. p. 293-300.

Atay SM, Kroenke CD, Sabet A, Bayly PV. Measurement of the Dynamic Shear Modulus of Mouse Brain Tissue In Vivo by Magnetic Resonance Elastography. J Biomech Eng. 2008; 130:21013.doi: 10.1115/1.2899575

Badachhape AA, Okamoto RJ, Durham RS, Efron BD, Nadell SJ, Johnson CL, Bayly PV. The Relationship of Three-Dimensional Human Skull Motion to Brain Tissue Deformation in Magnetic Resonance Elastography Studies. J Biomech Eng. 2017; 139:51002.doi: 10.1115/1.4036146

Bilston LE, Liu Z, Phan-Thien N. Large strain behaviour of brain tissue in shear: some experimental data and differential constitutive model. Biorheology. 2001; 38:335–45. [PubMed: 11673648]

Bilston LE, Liu Z, Phan-Thien N. Linear viscoelastic properties of bovine brain tissue in shear. Biorheology. 1997; 34:377–385. DOI: 10.1016/S0006-355X(98)00022-5 [PubMed: 9640354]

Brands D, Bovendeerd P, Peters GWM. Large Shear strain dynamic behavior of in vitro porcine brain brain tissue and a silicone gel model material. Stapp Car Crash J. 2000; 44:249–260. [PubMed: 17458730]

Chatelin S, Constantinesco A, Willinger R. Fifty years of brain tissue mechanical testing: from in vitro to in vivo investigations. Biorheology. 2010; 47:255–76. DOI: 10.3233/BIR-2010-0576 [PubMed: 21403381]

Clayton EH, Garbow JR, Bayly PV. Frequency-dependent viscoelastic parameters of mouse brain tissue estimated by MR elastography. Phys Med Biol. 2011; 56:2391–2406. DOI: 10.1088/0031-9155/56/8/005 [PubMed: 21427486]

Clayton EH, Genin GM, Bayly PV. Transmission, attenuation and reflection of shear waves in the human brain. J R Soc Interface. 2012; 9:2899–2910. DOI: 10.1098/rsif.2012.0325 [PubMed: 22675163]

Feng Y, Clayton EH, Chang Y, Okamoto RJ, Bayly PV. Viscoelastic properties of the ferret brain measured in vivo at multiple frequencies by magnetic resonance elastography. J Biomech. 2013a; 46:863–870. DOI: 10.1016/j.jbiomech.2012.12.024 [PubMed: 23352648]

Feng Y, Okamoto RJ, Namani R, Genin GM, Bayly PV. Measurments of mechanical anisotropy in brain tissue and implications for transversely isotropic material models of white matter. J Mech Behav Biomed Maetr. 2013b; 23:117–132. DOI: 10.1016/j.jmbbm.2013.04.007.Measurements

Gefen A, Margulies SS. Are in vivo and in situ brain tissues mechanically similar? J Biomech. 2004; 37:1339–1352. DOI: 10.1016/j.jbiomech.2003.12.032 [PubMed: 15275841]

Hoge CW, McGurk D, Thomas JL, Cox AL, Engel CC, Castro CA. Mild Traumatic Brain Injury in U.S. Soldiers Returning from Iraq. N Engl J Med. 2008; 358:453–463. DOI: 10.1056/NEJMoa072972 [PubMed: 18234750]

Holbourn AHS. MECHANICS OF HEAD INJURIES. Lancet. 1943; 242:438–441. DOI: 10.1016/S0140-6736(00)87453-X

Hrapko M, van Dommelen JA, Peters GW, Wismans JS. The Influence of Test Conditions on Characterization of the Mechanical Properties of Brain Tissue. J Biomech Eng. 2008; 130:31003.doi: 10.1115/1.2907746

Hrapko M, van Dommelen JaW, Peters GWM, Wismans JSHM. The mechanical behaviour of brain tissue: large strain response and constitutive modelling. Biorheology. 2006; 43:623–36. [PubMed: 17047281]

Johnson CL, McGarry MDJ, Van Houten EEW, Weaver JB, Paulsen KD, Sutton BP, Georgiadis JG. Magnetic resonance elastography of the brain using multishot spiral readouts with self-navigated motion correction. Magn Reson Med. 2013; 70:404–412. DOI: 10.1002/mrm.24473 [PubMed: 23001771]

Johnson CL, Schwarb H, McGarry MDJ, Anderson AT, Huesmann GR, Sutton BP, Cohen NJ. Viscoelasticity of subcortical gray matter structures. Hum Brain Mapp. 2016; 37:4221–4233. DOI: 10.1002/hbm.23314 [PubMed: 27401228]

Klatt D, Hamhaber U, Asbach P, Braun J, Sack I. Noninvasive assessment of the rheological behavior of human organs using multifrequency MR elastography: a study of brain and liver viscoelasticity. Phys Med Biol. 2007; 52:7281–7294. DOI: 10.1088/0031-9155/52/24/006 [PubMed: 18065839]

Langlois JA, Rutland-Brown W, Wald MM. The Epidemiology and Impact of Traumatic Brain Injury. J Head Trauma Rehabil. 2006; 21:375–378. DOI: 10.1097/00001199-200609000-00001 [PubMed: 16983222]

Manduca A, Oliphant TE, Dresner MA, Mahowald JL, Kruse SA, Amromin E, Felmlee JP, Greenleaf JF, Ehman RL. Magnetic resonance elastography: Non-invasive mapping of tissue elasticity. Med Image Anal. 2001; 5:237–254. DOI: 10.1016/S1361-8415(00)00039-6 [PubMed: 11731304]

Miller K, Chinzei K, Orssengo G, Bednarz P. Mechanical properties of brain tissue in-vivo: experiment and computer simulation. J Biomech. 2000; 33:1369–1376. DOI: 10.1016/S0021-9290(00)00120-2 [PubMed: 10940395]

Muthupillai R, Lomas D, Rossman P, Greenleaf J, Manduca A, Ehman R. Magnetic resonance elastography by direct visualization of propagating acoustic strain waves. Science (80-). 1995; 269:1854–1857. DOI: 10.1126/science.7569924

Nicolle S, Lounis M, Willinger R. Shear properties of brain tissue over a frequency range relevant for automotive impact situations: new experimental results. Stapp Car Crash J. 2004; 48:239–258. [PubMed: 17230269]

Okamoto RJ, Clayton EH, Bayly PV. Viscoelastic properties of soft gels: comparison of magnetic resonance elastography and dynamic shear testing in the shear wave regime. Phys Med Biol. 2011; 56:6379–6400. DOI: 10.1088/0031-9155/56/19/014 [PubMed: 21908903]

Ommaya AK. Mechanical properties of tissues of the nervous system. J Biomech. 1968; 1:127–138. DOI: 10.1016/0021-9290(68)90015-8 [PubMed: 16329300]

Papazoglou S, Hamhaber U, Braun J, Sack I. Algebraic Helmholtz inversion in planar magnetic resonance elastography. Phys Med Biol. 2008; 53:3147–3158. DOI: 10.1088/0031-9155/53/12/005 [PubMed: 18495979]

Rashid B, Destrade M, Gilchrist MD. Mechanical characterization of brain tissue in compression at dynamic strain rates. J Mech Behav Biomed Mater. 2012; 10:23–38. DOI: 10.1016/j.jmbbm.2012.01.022 [PubMed: 22520416]

Riek K, Klatt D, Nuzha H, Mueller S, Neumann U, Sack I, Braun J. Wide-range dynamic magnetic resonance elastography. J Biomech. 2011; 44:1380–1386. DOI: 10.1016/j.jbiomech.2010.12.031 [PubMed: 21295305]

Sack I, Beierbach B, Wuerfel J, Klatt D, Hamhaber U, Papazoglou S, Martus P, Braun J. The impact of aging and gender on brain viscoelasticity. Neuroimage. 2009a; 46:652–657. DOI: 10.1016/j.neuroimage.2009.02.040 [PubMed: 19281851]

Sack I, Rump J, Elgeti T, Samani A, Braun J. MR elastography of the human heart: Noninvasive assessment of myocardial elasticity changes by shear wave amplitude variations. Magn Reson Med. 2009b; 61:668–677. DOI: 10.1002/mrm.21878 [PubMed: 19097236]

Sack I, Streitberger K-J, Krefting D, Paul F, Braun J. The Influence of Physiological Aging and Atrophy on Brain Viscoelastic Properties in Humans. PLoS One. 2011; 6:e23451.doi: 10.1371/journal.pone.0023451 [PubMed: 21931599]

Schmidt JLL, Tweten DJJ, Benegal ANN, Walker CHH, Portnoi TEE, Okamoto RJJ, Garbow JRR, Bayly PVV. Magnetic resonance elastography of slow and fast shear waves illuminates differences in shear and tensile moduli in anisotropic tissue. J Biomech. 2016; 49:1042–1049. DOI: 10.1016/j.jbiomech.2016.02.018 [PubMed: 26920505]

Schregel K, Wuerfel nee Tysiak E, Garteiser P, Gemeinhardt I, Prozorovski T, Aktas O, Merz H, Petersen D, Wuerfel J, Sinkus R. Demyelination reduces brain parenchymal stiffness quantified in vivo by magnetic resonance elastography. Proc Natl Acad Sci. 2012; 109:6650–6655. DOI: 10.1073/pnas.1200151109 [PubMed: 22492966]

Shen F, Tay T, Li J, Nigen S, Lee P, Chan H. Modified Bilston Nonlinear Viscoelastic Model for Finite Element Head Injury Studies. J Biomech Eng. 2006; 128:797.doi: 10.1115/1.2264393 [PubMed: 16995770]

Sierra H, Cordova M, Chen C-SJ, Rajadhyaksha M. Confocal Imaging–Guided Laser Ablation of Basal Cell Carcinomas: An Ex Vivo Study. J Invest Dermatol. 2015; 135:612–615. DOI: 10.1038/jid.2014.371 [PubMed: 25178106]

Sinkus R, Tanter M, Xydeas T, Catheline S, Bercoff J, Fink M. Viscoelastic shear properties of in vivo breast lesions measured by MR elastography. Magn Reson Imaging. 2005; 23:159–165. DOI: 10.1016/j.mri.2004.11.060 [PubMed: 15833607]

Smith SM, Jenkinson M, Woolrich MW, Beckmann CF, Behrens TEJJ, Johansen-Berg H, Bannister PR, De Luca M, Drobnjak I, Flitney DE, Niazy RK, Saunders J, Vickers J, Zhang Y, De Stefano N, Brady JM, Matthews PM. Advances in functional and structural MR image analysis and implementation as FSL. Neuroimage. 2004; 23:S208–S219. DOI: 10.1016/j.neuroimage.2004.07.051 [PubMed: 15501092]

Thibault KL, Margulies SS. Age-dependent material properties of the porcine cerebrum: effect on pediatric inertial head injury criteria. J Biomech. 1998; 31:1119–1126. [PubMed: 9882044]

Tweten DJ, Okamoto RJ, Schmidt JL, Garbow JR, Bayly PV. Estimation of material parameters from slow and fast shear waves in an incompressible, transversely isotropic material. J Biomech. 2015; 48:4002–4009. DOI: 10.1016/j.jbiomech.2015.09.009 [PubMed: 26476762]

van Dommelen JAW, van der Sande TPJ, Hrapko M, Peters GWM. Mechanical properties of brain tissue by indentation: Interregional variation. J Mech Behav Biomed Mater. 2010; 3:158–166. DOI: 10.1016/j.jmbbm.2009.09.001 [PubMed: 20129415]

Vappou J, Breton E, Choquet P, Goetz C, Willinger R, Constantinesco A. Magnetic resonance elastography compared with rotational rheometry for in vitro brain tissue viscoelasticity measurement. Magn Reson Mater Physics, Biol Med. 2007; 20:273–278. DOI: 10.1007/s10334-007-0098-7

Vappou J, Breton E, Choquet P, Willinger R, Constantinesco A. Assessment of in vivo and post-mortem mechanical behavior of brain tissue using magnetic resonance elastography. J Biomech. 2008; 41:2954–2959. DOI: 10.1016/j.jbiomech.2008.07.034 [PubMed: 18805534]

Appendix

A. Error Analysis

The table below summarizes differences between *in vivo* and *ex vivo* experiments and their possible effects.

Table A.1

Error analysis comparing *in vivo* and *ex vivo* experiments

Potential error source	Comments	*In vivo*	*Ex vivo*
Wave amplitude	Shear modulus is estimated from the wave length. Differences in wave amplitude should not directly affect modulus estimates. In both methods, waves had enough amplitude to produce visible shear waves. In the small-strain regime we do not expect modulus to depend on amplitude.	Wave amplitude ~1.5μm Strain amplitude ~$2x10^{-4}$	Wave amplitude ~15μm Strain amplitude ~$2x10^{-3}$
Dominant wave direction	Both methods produced shear wave polarization displacements perpendicular to the dominant fiber direction, oriented right-left, of the corpus callosum. Although the tissue is actuated in different anatomical directions, the tissue is actuated similarly relative to the dominant fiber axis in both situations.	Dominant actuation direction: anterior-posterior (AP)	Dominant actuation direction: superior-inferior (SI)
Temperature	Temperature difference could cause differences in tissue properties. However, cooling of viscoelastic tissue generally leads to stiffening, so the temperature difference is more likely to mask differences in stiffness between the (apparently stiffer) *in vivo* and softer *ex vivo* tissue. The fact that a difference is still observed tends to support the	Body temperature ~37°C	Room temperature ~21°C

Potential error source	Comments	*In vivo*	*Ex vivo*
	paper's conclusions that *in vivo* tissue is stiffer.		
Excitation method	Excitation differences created differences in propagation direction. *In vivo* waves were excited externally and propagated inward from the skull. *Ex vivo* waves were excited in the center of the tissue and propagated outward (the rod created an internal boundary which was removed through erosion of voxels). The direction of wave propagation should not have an effect since fiber orientation was similar.	External actuation of skull by vibration of jaw	Axial excitation by central rod embedded in tissue
Voxel size	Voxel size affects the physical size of the estimation kernel for LDI, and the size of the eroded regions at boundaries. Kernel size does affect parameter estimates. Estimates converge as kernel size increases; kernel size is limited by sample size. Estimated effect: Results vary 3–7% (*ex vivo*) and 7–10% (*in vivo*) between kernel sizes of 5x5x5 to 7x7x7 voxels.	1.5 mm^3 isotropic voxels	1 mm^3 isotropic voxels
Boundary conditions	Boundary conditions are different, but comparable. The *in vivo* brain is surrounded by cerebrospinal fluid (CSF) and the skull. The *ex vivo* brain is surrounded in gelatin/glycerol and a hard plastic case. The boundaries should have only small effects on the conclusions of the study for two reasons: (1) In both cases, we analyzed interior ROIs, removed from the boundaries. All results are based on these interior ROIs. (2) Observed differences in estimated properties are greater at higher frequencies (with short wavelengths) at which the effects of boundaries are less likely to be important than at lower frequencies (longer wavelengths).	Skull and cerebral spinal fluid (CSF)	Gelatin/glycerol and plastic cylinder case

B. Linear Mixed Model

The multivariate regressions of storage modulus (G') and loss modulus (G'') were performed (Matlab R2017, Statistics Toolbox) using a linear mixed-effects model with random subject effects and fixed effects of group (*in vivo* vs. *ex vivo*) and frequency in the form:

$$y_i = a + b_1 x_{1i} + b_2 x_{2i} + b_3 x_{1i} x_{2i}. \quad \text{(B.1)}$$

In this model, y_i is G' or G'', a is the intercept, b_1 is the slope of the group variable, x_{1i} is the value of the group variable, b_2 is the slope of the frequency variable, x_{2i} is the value of the frequency variable, and b_3 is the slope of the interaction between group and frequency. The value of the group variable defines whether the tissue is *in vivo* ($x_{1i} = 1$) or *ex vivo* ($x_{1i} = 0$). Tables B.1 and B.2 outline the results of the analysis of G' and G'', respectively. The slopes between G' *in vivo* and *ex vivo* were significantly different ($p < 0.0001$) and frequency was a good predictor of the data ($p < 0.0001$). No significant differences were observed between G'' *in vivo* and *ex vivo* over this frequency range ($p = 0.285$). The linear mixed-effects model is plotted with G' and G'' estimates in Figure 8.

Table B.1

Results of multivariate regression of storage modulus (G') using a linear mixed-effects model with random subject effects

Effect	Variable	Estimate	Standard Error	Alpha (lower, upper)	P
Intercept	a	0.361	0.128	0.05 (0.102, 0.620)	0.007
Group	b_1	−0.926	0.178	0.05 (−1.283, −0.568)	<0.0001
Frequency (Hz)	b_2	0.0140	0.0007	0.05 (0.0126,0.0154)	<0.0001
Group*Frequency	b_3	0.0143	0.0016	0.05 (0.0110,0.0176)	<0.0001

Table B.2

Results of multivariate regression of loss modulus (G'') using a linear mixed-effects model with random subject effects

Effect	Variable	Estimate	Standard Error	Alpha (lower, upper)	P
Intercept	a	−0.309	0.070	0.05 (−0.448, 0.167)	<0.0001
Group	b_1	−0.108	0.100	0.05 (−0.310, −0.093)	0.285
Frequency (Hz)	b_2	0.00592	0.00035	0.05 (0.00522,0. 0.00662)	<0.0001
Group*Frequency	b_3	0.00324	0.00091	0.05 (0.00140,0.00508)	0.0009

C. Summary of Rheological Model Fitting

Several rheological models were fitted to the complex shear modulus estimates from both *in vivo* and *ex vivo* data. Classic rheological models do not fit the estimated moduli well (Table C.1), possibly due to poroelastic behavior (McGarry et al., 2015). However, as noted by Testu et al. (2017), dual power-law models fitted separately to G' and G'' fit the frequency-dependent shear moduli much better than the classic (springpot) power-law.

Table C.1

Summary of rheological data fitting.

Model	In vivo		Ex vivo	
	Parameters	R^2	**Parameters**	R^2
Power law (dual)[#] $G' = k_1\omega^{a1}$ $G'' = k_2\omega^{a2}$	$k_1 = 2.88 \times 10^{-4}$ $a_1 = 1.39$ $k_2 = 8.60 \times 10^{-9}$ $a_2 = 2.75$	0.924	$k_1 = 7.93 \times 10^{-3}$ $a_1 = 0.840$ $k_2 = 2.11 \times 10^{-5}$ $a_2 = 1.48$	0.940
Power law (springpot)[†] $G^* = k(i\omega)^{\alpha}$	$k = 0.490$ $\alpha = 0.214$	0.168	$k = 0.563$ $\alpha = 0.253$	0.357
Zener[‡] $G^* = G_\infty \frac{1+d(i\omega\tau)}{1+i\omega\tau}$	$G_\infty = 1.09$ $d = 2.38$ $\tau = 1.77 \times 10^{-3}$	0.257	$G_\infty = 1.93$ $d = 2.58$ $\tau = 6.61 \times 10^{-4}$	0.515
Fractional Zener[‡] $G^* = G_\infty \frac{1+d(i\omega\tau)^{0.5}}{1+i\omega\tau}$	$G_\infty = 0.473$ $d = 7.88$ $\tau = 9.64 \times 10^{-4}$	0.178	$G_\infty = 0.722$ $d = 10.89$ $\tau = 2.60 \times 10^{-4}$	0.377
Generalized Maxwell[§] $G^* = G_\infty + \frac{i\omega\tau_1 G_1}{1+i\omega\tau_1} + \frac{i\omega\tau_2 G_2}{1+i\omega\tau_2}$	$G_\infty = 1.09$ $G_1 = 3.00 \times 10^{-15}$ $G_2 = 1.51$ $\tau_1 = 2.84 \times 10^{-5}$ $\tau_2 = 1.77 \times 10^{-3}$	0.257	$G_\infty = 1.93$ $G_1 = 3.14 \times 10^{-14}$ $G_2 = 3.05$ $\tau_1 = 3.48 \times 10^{-5}$ $\tau_2 = 6.61 \times 10^{-4}$	0.515

Units: *Power law: k*, k_1, k_2 (kPa-s$^{\alpha}$), α (non-dimensional). *Zener, fractional Zener, and generalized Maxwell:* G_∞, G_1 G_2 (kPa); d (non-dimensional); τ, τ_1, τ_2 (sec).

[#](Testu et al., 2017);

[†](Koeller et al, 1984);

[‡](Kohandel et al., 2005);

[§](Flugge, 1967)

References

Flugge, W. Viscoelasticity. Blaisdell Publishing Company; Waltham, Massachusetts: 1967.

Koeller RC. Applications of fractional calculus to the theory of viscoelasticity. J Appl Mech. 1984; 51:299–307.

Kohandel M, Sivaloganathan S, Tenti G, Darvish K. Frequency dependence of complex moduli of brain tissue using a fractional Zener model Phys. Med Biol. 2005; 50:2799–805.

McGarry MD, Johnson CL, Sutton BP, Georgiadis JG, Van Houten EE, Pattison AJ, Weaver JB, Paulsen KD. Suitability of poroelastic and viscoelastic mechanicalmodels for high and low frequency MR elastography. Med Phys. 2015; 42(2):947–57. [PubMed: 25652507]

Testu J, McGarry MDJ, Dittmann F, Weaver JB, Paulsen KD, Sack I, Van Houten EEW. Viscoelastic power law parameters of in vivo human brain estimated by MR elastography. J Mech Behav Biomed Mater. 2017; 74:333–341. [PubMed: 28654854]

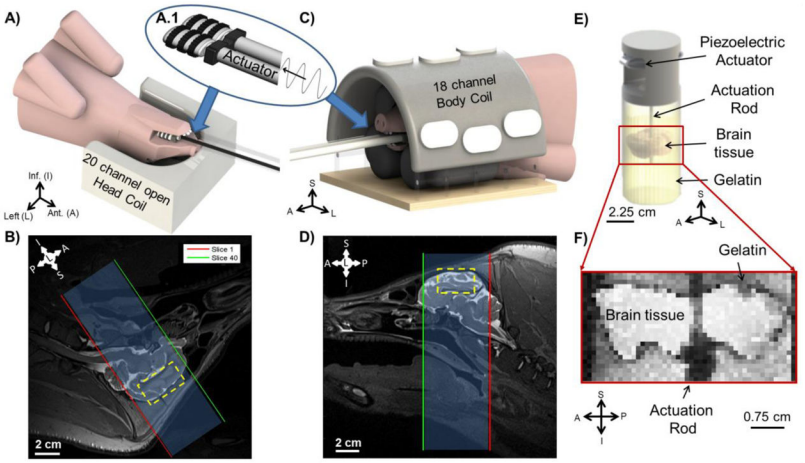

Figure 1.

A–D) Experimental set-up for MRE *in vivo*. A custom actuator (A.1) driven by the Resoundant™ system is placed between the back molars of the mini-pig jaw to induce vibrations in the skull and shear waves in brain at 50, 80, 100, and 125 Hz while the mini-pig is positioned in dorsal recumbency or ventral recumbency. A) Mini-pig scanned in dorsal recumbency with its head placed in the lower part of the Seimens Head/Neck20 coil. Padding and Velcro™ secured the head from excess motion. B) T2-weighted anatomical image (sagittal view, 0.8 mm^3 voxels) of the mini-pig in dorsal recumbency, with MRE slices highlighted. Yellow rectangle shows the approximate location of the *ex vivo* brain tissue disk. C) Mini-pig scanned in ventral recumbency with its head placed under a custom, half-dome, Plexiglas frame which supported the Siemens 18-Channel Body Matrix Coil. Padding and Velcro™ secured the head from excess motion. D) T2-weighted anatomical image (sagittal view, 0.8 mm^3 voxels) of mini-pig in ventral recumbency, with MRE slices highlighted. Yellow rectangle shows approximate location of *ex vivo* brain tissue disk. E–F) Experimental set-up for MRE *ex vivo*. E) The cylindrical brain tissue sample is embedded in gelatin and excited by a central actuation rod at 80, 100, 125, 200, and 300 Hz using a piezoelectric actuator. F) Anatomical image (1 mm^3 voxels) of the *ex vivo* brain tissue sample and gelatin, TE = 60 ms and TR = 1000 ms.

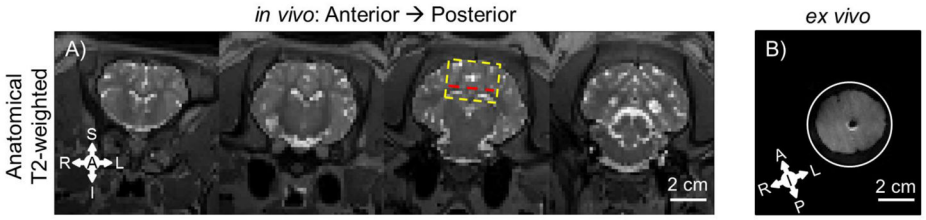

Figure 2.

Comparison of experimental data from the porcine brain *in vivo* (A) and *ex vivo* (B). A) T2-weighted MR images of four non-contiguous (7.5 mm spacing) coronal slices of the brain *in vivo* at 1.5 mm resolution. Yellow rectangle shows approximate location of *ex vivo* brain tissue disk. Red line denotes approximate slice location pictured in B. B) T2-weighted image of *ex vivo* cylindrical sample from the same animal at 1 mm resolution.

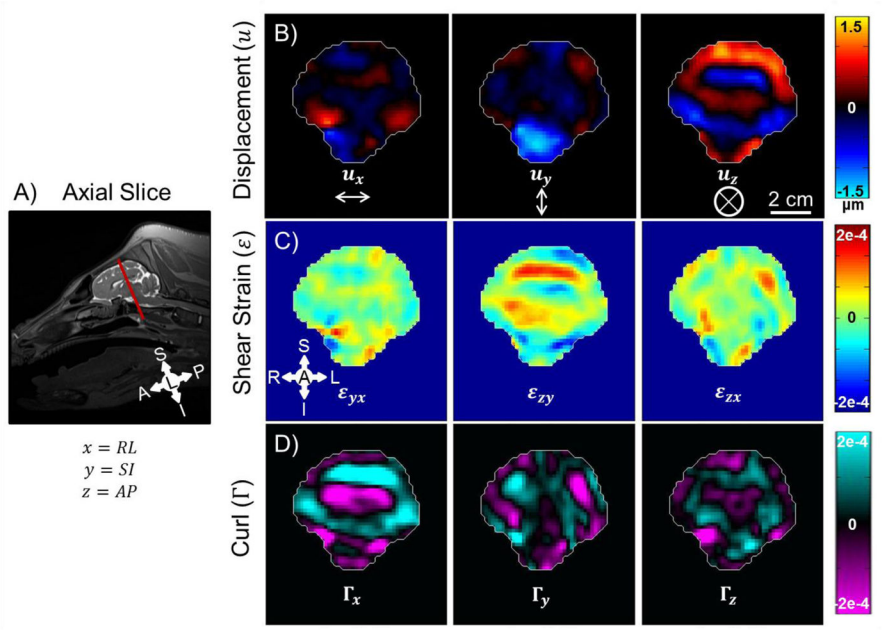

Figure 3.

In vivo MRE results for one axial slice of mini-pig brain at 100 Hz imaged while positioned in dorsal recumbency. A) Image slice location. B) Three components of displacement. C) Three components of shear strain. D) Three components of curl.

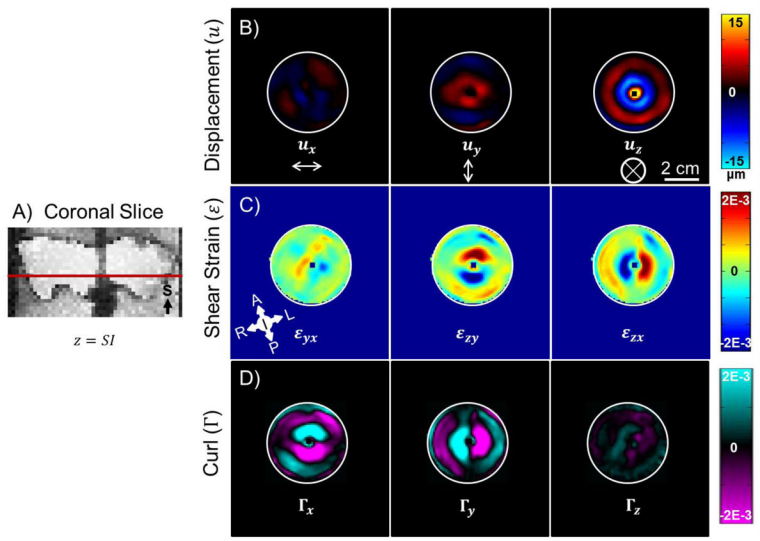

Figure 4.

Ex vivo MRE results for one axial slice of brain tissue at 100 Hz. A) Image slice location. Images are from the same mini-pig shown in Figure 3. B) Three components of displacement. C) Three components of shear strain. D) Three components of curl. Note orientations and scale bars are different from Figure 3.

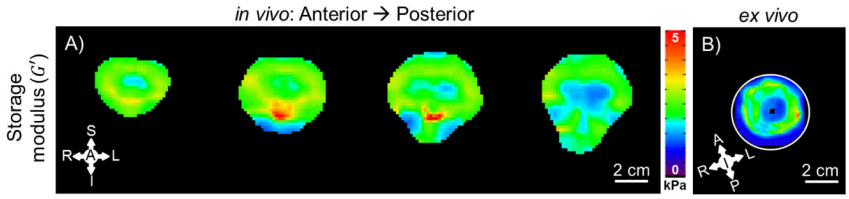

Figure 5.

A) Storage modulus (G') at 100 Hz *in vivo* estimated using LDI. The AP component of motion is shown for the same image slices as in Figure 3A and B. G' was only estimated for voxels where >50% of the 7x7x7 fitting kernel was inside the brain. B) Storage modulus (G') at 100 Hz *ex vivo* estimated using LDI. The SI component of motion is shown for the same image slice as in Figure 3C and D. G' was only estimated for voxels where >50% of the 7x7x7 fitting kernel was inside the sample. Note: Image scales are the same in each panel (scale bars = 2 cm), but image slice orientations differ between panels A and B.

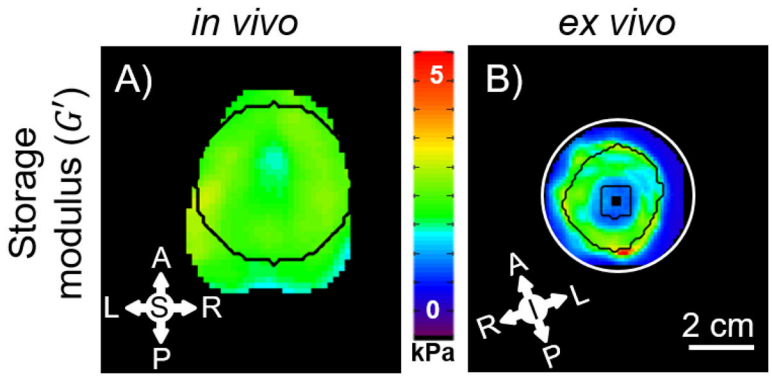

Figure 6.

LDI-estimated storage modulus (G') for one *in vivo* (A) and one *ex vivo* (B) mini-pig coronal brain slice using 7x7x7 kernel for LDI. Black outlines denote the area used in the comparison between *in vivo* and *ex vivo* samples. The *ex vivo* sample was eroded using a 7x7x7 kernel to remove the influence of gelatin on G' estimates.

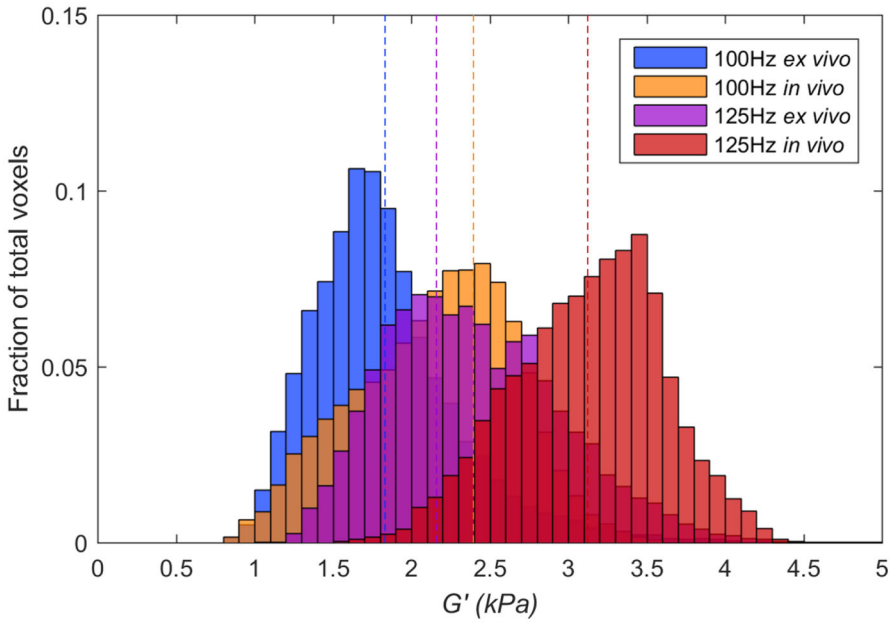

Figure 7.

Histogram of LDI-estimated storage modulus (G') values of all pixels for *in vivo* (orange and red) and *ex vivo* (blue and purple) calculated at 100 and 125 Hz using a 7x7x7 kernel for all of the scanned mini-pigs. Dotted lines represent the mean G' value. *In vivo* voxels are from the cylindrical ROI shown in Figure 6A. *Ex vivo* voxels are from the eroded ROI shown in Figure 6B.

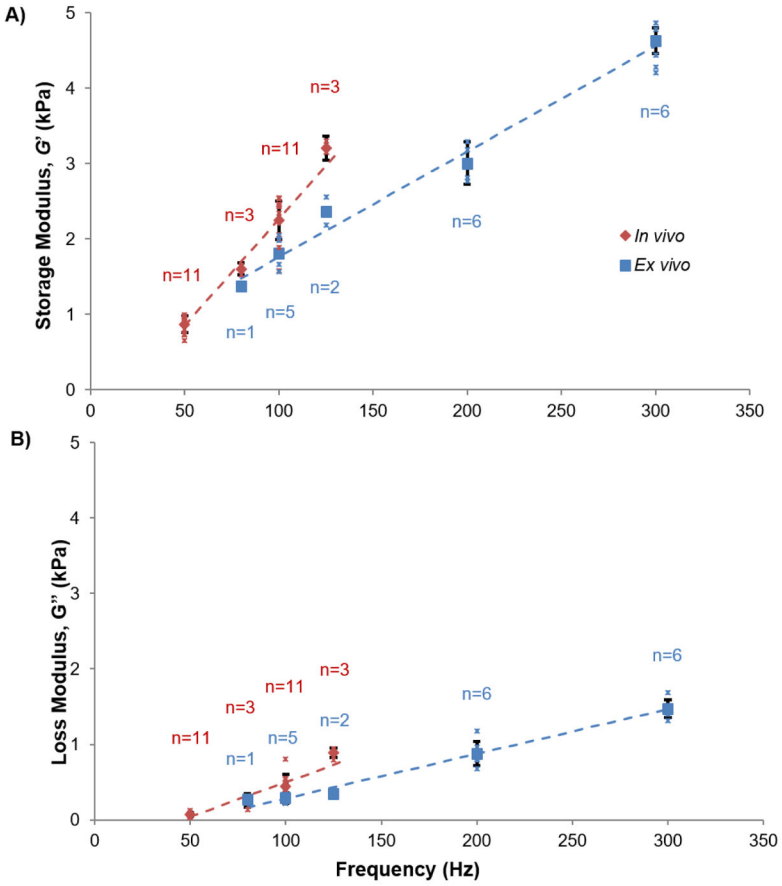

Figure 8.

Mean storage modulus (G') and loss modulus (G'') of *in vivo* (red) and *ex vivo* (blue) mini-pig brain tissue estimated by LDI at frequencies from 50–300 Hz for N=6 animals. Each small asterisk (*) represents the mean G' or G'' for one mini-pig scanned at the specified frequency. Each larger marker (blue □ and red ◇) represents the mean G' or G'' for all mini-pigs scanned at the specified frequency. Notations above/below markers provide the number of scans represented by the mean value. Standard deviations were only provided for data sets with n≥3. For *in vivo* data, each marker shows the average modulus estimate in a cylindrical ROI of dimensions matching that of the *ex vivo* cylindrical sample (Figure 1B). Multivariate linear regressions of G' and G'' were performed using a linear mixed-effects model with subject as a random effect (dashed lines; see Appendix B). *In vivo:* $G' = 0.85 + 0.0283\,(f - 50)$; $G'' = 0.041 + 0.00916\,(f - 50)$. *Ex vivo:* $G' = 1.48 + 0.0140\,(f - 80)$; $G'' = 0.164 + 0.00592\,(f - 80)$. A) Estimates of G' increase with frequency due to viscoelasticity. At the common frequencies, 80, 100, and 125 Hz, G' estimates are higher for brain tissue *in vivo* than for brain tissue samples *ex vivo*. B) Estimates of G'' increase with frequency due to viscoelasticity.

Table 1

Numbers of anatomical and MRE scans performed *in vivo* and *ex vivo* in the 6 mini-pigs.

	T1/T2	MRE 50 Hz	MRE 80 Hz	MRE 100 Hz	MRE 125 Hz	MRE 200 Hz	MRE 300 Hz
In vivo	19	11	2	10	3	-	-
Ex vivo	6	-	1	5	2	6	6